Competing influences of greenhouse warming and aerosols on Asian Summer Monsoon circulation and rainfall

William K.M. Lau[1,2]

Kyu-Myong Kim[3]

[1] *Earth System Science Interdisciplinary Center, U. of Maryland*

College Park, MD 20740

[2] *Texas A&M University, Station College, Texas, 77843*

[3] *Climate and Radiation Laboratory, NASA/Goddard Space Flight Center*

Greenbelt, MD 20771

Submitted to APJAS

Revised March 2017

Abstract

In this paper, we have compared and contrasted competing and amplifying influences on the global and regional drivers, circulation and rainfall responses of the Asian monsoon under global greenhouse warming (GHG) and aerosol forcing, based on CMIP5 historical simulations. Under GHG-only forcing, the land warms much faster than the ocean, magnifying the pre-industrial climatological land-ocean thermal contrast and hemispheric asymmetry, *i.e.,* warmer northern than southern hemisphere. A steady increasing warm-ocean-warmer-land (WOWL) trend has been in effect since the 1950's substantially increasing moisture transport from adjacent oceans, and enhancing rainfall over the Asian monsoon regions. However, under GHG warming, increased atmospheric stability due to strong reduction in mid-tropospheric and near surface relative humidity coupled to an expanding subsidence areas, associated with the Deep Tropical Squeeze (DTS, Lau and Kim, 2015b) strongly suppress monsoon convection and rainfall over subtropical and extratropical land, leading to a weakening of the Asian monsoon meridional circulation. The inclusion of aerosol emissions strongly masks WOWL, by over 60% over the northern hemisphere, negating to a large extent the rainfall increase due to GHG warming, and leading to a further weakening of the monsoon circulation, through increasing atmospheric stability, most likely associated with aerosol solar dimming and semi-direct effects. Overall, we find that GHG exerts stronger positive rainfall sensitivity, but less negative circulation sensitivity in SASM compared to EASM. In contrast, aerosols exert stronger negative impacts on rainfall, but less negative impacts on circulation in EASM compared to SASM.

1. Introduction

According to the 5th Assessment Report, Inter-governmental Panel on Climate Change (IPCC 2013), global monsoon rainfall is likely to increase, while the monsoon circulation to weaken in a warmer climate. The enhanced monsoon rainfall has been attributed to increased land-sea contrast, and more abundant precipitable water in a warmer climate, while the decreased monsoon circulation is associated with an overall weakening of the large-scale circulation required for global water balance under greenhouse gases (GHG) warming (Turner and Annamalai, 2012; Wang et al., 2012). In recent decades, while the Asian monsoon has experienced an apparent weakening in winds, it also has witnessed a general decrease in monsoon rainfall over India and persistent drought condition over northern China in conjunction with heavy rain in southern China *i.e.,* the so–called North-Dry-South-Wet (NDSW) pattern (Yu et al.,2004, 2007, Zhou et al., 2009, Lau and Kim, 2015a; Li et al., 2016). The weakening of Asian monsoon circulation and rainfall reduction have been attributed variously to aerosol effects, sea surface temperature changes arising from GHG warming and aerosols, as well as multi-decadal natural variability (Chung and Ramanathan, 2006; Ramanathan and Carmichael, 2008; Ding et al., 2008; Zhou et al*.,* 2008; Liu et al*.*, 2009; Cowan and Cai, 2011; Ganguly et al., 2012; Annamalai et al., 2013; Bollasina et al*.,* 2011, 2014; Wang et al., 2013b; Lee and Wang, 2014; Cheng and Zhou, 2014, Polson et al., 2014, Lau and Kim, 2015a; Roxy et al., 2015). On the other hand, studies have also shown that aerosols can enhance monsoon deep convection and rainfall through aerosol-cloud interactions (Rosenfeld et al., 2008; Fan et al., 2013; Li et al., 2016), and that absorbing aerosol effect can lead to increased or re-distribution of Indian monsoon rainfall depending on aerosol

63 types with different optical and physical properties, via induced dynamical feedback
64 processes, such as the Elevated Heat Pump (EHP) and related mechanisms, during different
65 phases of the monsoon season (Lau et al., 2006, 2008; Lau and Kim, 2006, 2010; Meehl et
66 al., 2008; Randles and Ramaswamy, 2008; Wang et al., 2009; Ye et al., 2013).
67 Additionally, modeling studies have shown that the responses to the same global climate
68 change forcing from GHG and aerosols are quite different between the South Asian Summer
69 Monsoon (SASM) and the East Asian Summer Monsoon (EASM) (Menon et al., 2002; Wang
70 et al., 2013b; Zhang et al., 2009; Song et al., 2014, Li et al., 2015, Zhang and Li, 2016).
71 Because of the diverse model results and difficulty in matching long-term observations and
72 model results, unraveling the relative roles of GHG warming, aerosols, natural variability,
73 local feedback processes and differences between the SASM and EASM forcing and
74 responses remain a major challenge. The objective of this work is to seek a more
75 fundamental understanding of climate change in the Asian monsoon regions by examining
76 the competing influences of GHG and aerosol forcing on key global and large-scale controls
77 of the entire Asian monsoon, and then elucidate differences in regional forcing and
78 feedback responses to changes in these controls.
79

80 **2. Approach and Basic Concepts**

81 Up to now, a commonly used approach for observational and modeling studies of
82 climate change in Asian monsoon regions has focused on examining changes in rainfall and
83 circulation patterns over pre-selected sub-domains within the monsoon region, usually for
84 a limited duration ($\lesssim$ 50 years). Because of the limited space-time domains chosen, the
85 difficulty in separating the myriad climate forcing (local or remote, natural and

86 anthropogenic) and the complex regional feedback processes is compounded. More often
87 then not, these studies were carried out separate for the SASM and EASM, and did not
88 include comparing and contrasting the regional forcing and responses of the two regional
89 monsoons. In this work, we first investigate the global, zonally symmetry, and asymmetric
90 forcing by greenhouse gases and aerosols with regard to their impacts on land-sea thermal
91 contrast, relative humidity, moisture transport, and moist static energy on the Asian
92 monsoon as a whole. Then we compare and contrast the regional forcing and responses in
93 circulation and rainfall in the context of changes in these global forcing, for the SASM and
94 EASM respectively.
95 Results are based on CMIP5 historical runs for 135 years (1870-2005) under various
96 prescribed emission scenarios: 1) all forcing (ALL) including prescribed GHG, aerosol
97 emissions from historical inventories, and natural variability representing changes in solar
98 irradiance and aerosol emission from historical volcanic eruptions, 2) GHG-only, or simply
99 GHG , and 3) natural variability only. To focus on the "forced" response of the Asian
100 monsoon due to emission changes, we have minimized the impacts of model natural
101 internal variability, by constructing the Multi-Model-Mean (MMM) from an ensemble of 19
102 CMIP5 models, for all the key quantities for the June-July-August (JJA) seasonal mean. A
103 model anomaly is defined as the difference between the MMM of the last 25 years (1981-
104 2005) of the model integration, with respect to the pre-industrial (PI) control. The MMM
105 outputs for GHG-only will be used to establish the baseline of climate forcing and responses
106 of the Asian monsoon. By comparing GHG to ALL, the degree to which GHG forcing and
107 responses are masked or modulated by aerosols will be estimated. The inferred
108 anthropogenic aerosol (IAA) effect (including nonlinearity) is obtained by subtracting GHG

and NAT from ALL (ALL-GHG-NAT). The regional MMM rainfall and circulation responses are then examined in the context of changes of key global and regional forcing, and local feedback processes respectively for the SASM and EASM, based on comparison of the GHG, ALL, and IAA. All models outputs have been interpolated to a global a 2.5° x 2.5° latitude-longitude common grid. Reliability of model results is measured by a consistency test defined at each grid point, by the percentage of models with anomalies having the same sign as the MMM anomaly exceeding given thresholds (IPCC 2013). We use two consistency thresholds, 75% (15 out of 19 models) and 65% (13 out of 19 models) in this work. An assessment of the possible impacts of GHG v. aerosols forcing on Asian monsoon based on comparison of MMM rainfall anomaly to observations from APHRODITE (Yatagai et al., 2012) is also presented.

2.1 Basic concepts

To facilitate the discussion of results, we first present a rudimentary but important concept of heating balance in the tropics. In a moisture-rich tropical environment, typical of the monsoon, an approximate heat balance in the atmosphere is between diabatic heating, Q and adiabatic cooling by the large-scale vertical motion w, *i.e.,* $-w\Gamma_e \approx \frac{Q}{C_p}$, where Γ_e is the moist adiabatic lapse rate, C_p the heat capacity at constant pressure (Holton 1992). In monsoon regions, where generally the mean vertical motion is positive (w>0), and diabatic heating due mostly to latent heating, we have $Q \approx L_s P$, and $wM \approx P$, where $M = -\frac{C_p}{L_s}\Gamma_e$ is the moist stability parameter. Differentiating we have:

$$\frac{\Delta P}{P} \approx \frac{\Delta w}{w} + \frac{\Delta M}{M} \qquad (1)$$

where the first term on the right represents changes in dynamics, and the second term changes in thermodynamics. For increased (decreased) moist stability, $\Delta M < 0$ ($\Delta M > 0$). Eq (1) indicates that in monsoon regions, precipitation change is a function of both dynamics (circulation) and thermodynamics (moist stability). As such, increased precipitation can co-exist with a weakened monsoon circulation, provided moist stability is increased, or vice versa. Eq (1) will be used to quantify the relationship among circulation, rainfall and stability under GHG and aerosol forcing respectively, for the SASM and EASM (See Section 3.3c).

3. Results

In the next two sub-sections, we will examine the global forcing of the monsoon. For a given climate system, the total forcing F can be expressed as:

$$F(\phi, \lambda, z) = \bar{\bar{F}} + \bar{F}(\phi, z) + \tilde{F}(\phi, \lambda, z) \qquad (2)$$

where ϕ=latitude, λ=longitude, z= height, consisting of $\bar{\bar{F}}$, the global mean, $\bar{F}$, the zonally symmetric, and $\tilde{F}$, the zonally asymmetric components. Since the monsoon is driven by thermal contrasts, only the zonally symmetric, and asymmetric components are important. We will start with the zonally asymmetric component global forcing.

3.1 Land-Sea thermal contrast

It is well known that one of the main drivers of the monsoon is the large-scale land-sea thermal contrast (Lau and Li, 1984; Li and Yanai, 1996; Webster et al., 1998, and many others). An increase land-sea contrast will increase moisture transport from ocean to land over the Asian monsoon regions (See discussion Section 3.3). During JJA, under GHG, the

surface temperature rises everywhere, but with more warming over the land than the ocean, due to the much larger heat capacity of the ocean (Fig. 1a). The most pronounced warming is found over the extratropical land regions of northern Eurasia and North America and Greenland, around the Arctic Circle in northern hemisphere, and in the Antarctic because of strong ice-snow albedo feedback (Dickenson et al., 1987). Over the subtropical and tropical regions, the land areas of both hemispheres are also warmer than the surrounding oceans. Overall, the GHG warming is asymmetric, with stronger warming in the Northern Hemisphere (NH) than in the Southern Hemisphere (SH). Under ALL (Fig. 1b), the warming over both global land and oceans are more subdued compared to GHG, reflecting the "masking" effect by aerosols (Ramanathan and Feng, 2009). For quantitative comparison, we define the "aerosol masking effect" as:

$$AME = \left[1 - \frac{\Delta T_{S,ALL}}{\Delta T_{S,GHG}}\right] \quad (3)$$

where ΔT_S is the surface temperature for the GHG-only and ALL experiments respectively as indicated by the subscript. AME has been computed for land, and ocean, and for the northern (NH) and southern hemisphere (SH) separately (Table 1). Globally, AME is large, masking 58% and 49% of the GHG warming over land and ocean respectively. AME is stronger in NH (62 % for land, 62% for ocean) than the SH (45% for land, 36% for ocean), reflecting strong hemispheric asymmetry due to higher level of aerosol emission and loading in the NH. The importance of the hemispheric thermal asymmetry in driving the global monsoons of both hemispheres in terms of strong cross-equatorial moisture transport has been noted in previous studies (Wang et al., 2013a; Lee and Wang, 2014), and will be addressed in Section 3.3

177 Focusing on the differential warming between the land and ocean as a global
178 monsoon driver, we define a Warm-Ocean-Warmer-Land (WOWL) monsoon forcing as the
179 land-sea surface temperature difference 10^{o}S-30^{o}N. Under GHG, WOWL, averaged over the
180 last 25 years (1991-2005) of the model integration, increases by 0.42^{o} C relative to PI, with
181 the fastest rate (~0.07^{o} C per decade) during 1950-2005 (Fig.1c). Under ALL, the rate of
182 WOWL increase is much slower (~0.038^{o}C per decade) for the same period, culminating in
183 an increase of approximately 0.19^{o} C in the last 25 years compared to PI, indicating a strong
184 AME of approximately 54%. Natural variability (NAT) shows a weak negative WOWL
185 during the last 5 decades, possibly due to the enhanced land cooling by sulfate aerosols
186 injected from strong volcanic eruptions during this period (Robock, 2000, Man et al., 2014).
187 The IAA effect, obtained by subtracting NAT and GHG from All, shows a strong negative
188 WOWL during the last 25 years with a pronounced trend (~ - 0.0275°C per decade) since
189 1950, coinciding with the post-war rapid modernization of the modern era
190
191 *3.2 Global drying under GHG warming*
192 Recent observational and global climate model studies have suggested that GHG
193 warming is associated with overall drying of the subtropical and extratropical continents
194 (Dai 2006, 2011; Sherwood et al., 2010; Lau et al., 2013; Fu and Feng, 2014). Particularly
195 relevant to the ensuing analysis, Lau and Kim (2015b) has found that under GHG warming,
196 a characteristic signature in change of the global water cycle is an quasi-zonally symmetric
197 drying of the subtropical and extratropical mid- and-lower troposphere, in association with
198 a tightening of the ascending branch of the Hadley Circulation (HC), deeper convection over
199 the equatorial central and eastern Pacific, coupled to increased subsidence and widening of

200 the subtropical dry zone - the so-called Deep Tropical Squeeze (DTS) . We have computed
201 the tropospheric drying pattern for JJA in the form of a height-latitude zonally averaged
202 relative humidity (RH) anomalies under GHG and ALL forcing respectively (Fig. 2). Under
203 GHG-only forcing (Fig. 2a), the overall drying (δRH<0) in the upper troposphere in the deep
204 tropics, in the mid- and lower troposphere in the subtropics and mid-latitude are very
205 pronounced. In the northern hemisphere monsoon subtropics and mid-latitudes of major
206 continental land regions (20-50^{o}N), the drying extends downward to the earth surface. On
207 the other hand, moistening (δRH>0) in the lower troposphere and near the surface is found
208 over the deep tropics and polar region, in conjunction with increased precipitation over
209 these regions (Lau et al., 2013). Under GHG forcing, the warming of upper troposphere is
210 stronger compared to that of lower troposphere because of the moist adiabatic effect
211 (Holton, 1992). The reduction in RH can also be understood in terms of the Clausius
212 Clapyeron relationship, involving relative humidity:

213 $$\delta RH = \frac{\delta q}{q_s} - \alpha . RH . \delta T \qquad (4)$$

214 where $\alpha = L(R_v T^2)^{-1} \sim 6.5\%\ K^{-1}$, and q_s is the saturated vapor pressure, R_v the ideal gas
215 constant, and T is the ambient temperature. From Eq (4), it can readily be deduced that a
216 faster increase in temperature compared to increase in moisture can lead to a reduction in
217 RH. This is the reason for strong RH reduction in the lower troposphere and near the
218 surface in the northern hemisphere subtropics and mid-latitudes (25-50^{o}N) under GHG
219 warming, because of presence of much warmer continental land mass over these latitudes.
220 The increase in RH near the tropopause and above is contributed by the warming of the
221 troposphere and cooling of the stratosphere – a fingerprint of the GHG warming (Santers

et al., 2012). Under All (Fig. 2b), the GHG warming fingerprint in RH is still discernable, but weaker overall, reflecting strong AME due to aerosols.

The spatial patterns of the RH anomaly, in relations to SST and global circulation anomalies under GHG and ALL are discussed next. As shown in Fig. 3a, the 500 hPa RH anomaly pattern is indeed quasi-zonally symmetric and global in extent, characterized by a narrow band of increased RH over the near-equatorial regions, most pronounced over the Pacific, the Atlantic and central Africa, coupled to regions of strong mid-troposphere drying ($\delta RH<0$), and large-scale mid-troposphere anomalous descending motions, poleward of $30^{o}N$ and $20^{o}S$. The most pronounced reduction in RH is found over the Southern Hemisphere subtropics ($\sim 30^{o}$ S), which co-locates with the major descending branch of the HC during boreal summer. Over the northern hemisphere, the strongest RH reduction is found over the subtropical and extratropical land masses of Eurasia, northeastern Asia, and northern North American. RH is also reduced over the equatorial Indian Ocean, Bay of Bengal, southeast Asia, and southern China, where mid-troposphere anomalous descending motions prevail. This occurs in conjunction with a weakening of the Walker Circulation under GHG warming (see discussion for Fig. 3d), consistent with previous studies (Vecchi and Soden, 2007; Tokinaga et al., 2012). At 850hPa (Fig. 3b), the RH-reduction regions appears to further "squeeze" toward the equator, with more pronounced and widespread drying ($\delta RH<0$) over the tropics and subtropics land regions of East Asia southern Europe/North Africa, as well as the Americas, and adjacent oceanic regions, while the RH-enhancement zones become narrower over the equatorial Pacific and central Africa/Middle East region. The narrowing of the zone of increased 850hPa RH is consistent with the DTS, characterized by increased subsidence on both immediate sides of the narrow zone (Fig.

245 3b), in conjunction with the development of an east-west oriented, narrow warm sea
246 surface temperature (SST) tongue (Fig. 3c) over the central and eastern equatorial Pacific.
247 The SST anomaly signals a reduced climatological east-west SST gradient along the
248 equator, which is physically consistent with a weakened Walker Circulation, featuring
249 anomalous ascent over the equatorial central and eastern Pacific, and descent over the
250 Indian Ocean and Maritime Continent region (Fig. 3d). The widespread RH reduction and
251 anomalous subsidence in the mid-lower troposphere will suppress deep convection and
252 clouds, opposing the tendency for increased rainfall favored by increased low-level
253 moisture transported from ocean to land under GHG (See discussion in Section 3.3 and 3.4).
254 Under All, the RH anomalous patterns are similar to GHG-only with widespread
255 tropospheric drying over tropical and extratropical land and oceans at 500hPa (Fig. 3e)
256 and at 850hPa (Fig. 3f), except that wet-dry contrast is relatively weaker, with the zone of
257 positive RH near the equator broader and less well-defined compared to GHG. Likewise,
258 the SST warm tongue and east-west SST gradient (Fig. 3g), and the anomalous rising
259 motion over the equatorial central Pacific (Fig.3h) are much less developed. These signal a
260 relatively muted development of the DTS, and reduced influence of the Walker Circulation
261 compared to GHG. Notably, over the Asian monsoon regions, under ALL, compared to GHG
262 (Fig. 3a), the mid- and lower troposphere is even drier with expanded areas of anomalous
263 subsidence (Fig. 3e), and the anomalous subsidence over the Indian Ocean and Maritime
264 continent have intensified (Fig 3h), reflecting a strong stabilizing effect of aerosols on the
265 monsoon circulation in these regions (Bollasina et al., 2011; Lau and Kim, 2015a).
266
267 *3.3 Asian monsoon regional responses*

The regional responses of the Asian monsoon for the SASM and EASM are assessed in light of the large-scale monsoon forcing described in previous sections.

a. Moisture transport

Under GHG, the Indian Ocean and tropical Western Pacific reach a much higher level of total precipitable water (TPW) due to the warmer SST, and much stronger anomalous moisture transport from ocean to the Asian monsoon land stemming from stronger WOWL, compared to ALL (Fig. 4). The Indian subcontinent and the Bay of Bengal are moistened by increased southwesterly moisture transport which appears to originate from the confluence of two distinct transport streams (Fig. 4a). First and foremost is the strengthening of the Somali Jet along the coast of East Africa, accompanied by strong cross-equatorial flow, along 40-60^{o}E, likely due to the stronger warming of the NH compared to the SH (referred to Fig. 1 and Table 1). Second is the increased westerly moisture transport over central Africa (5 -15^{o} N), from the warmer equatorial Atlantic Ocean (see Fig. 3c). The southwesterly moisture transport turns sharply into southerly transport over southern and central China, reaching northeastern China, Korean and Japan. Here, the increased southerly transport may also be contributed from increased TPW over the tropical western Pacific warm pool associated with a strengthening of the Western Pacific Subtropical High under GHG warming (Song et al., 2014). Interestingly, anomalous northerly moisture transport is found over the northwestern Asia including eastern Eurasia toward the Asian monsoon region, implying a drying tendency over northwestern Asia, and northern Eurasia. This northerly transport coincides with regions of anomalous subsidence, and reduced RH in the mid- and lower troposphere under GHG warming (See Fig. 3). Under All (Fig. 4b), the pattern of ocean-to-land moisture transport is similar to

GHG-only, except the magnitude is substantially reduced, due to the weakening WOWL by aerosol masking effect.

Table 2 summarizes the changes in 850hPa moisture flux across the different key cross-sections of the SASM and EASM (See Fig. 4a for geographic locations of cross-sections). Here a positive sign denotes westerly or southerly transport as appropriate for each cross section. For SASM, the PI climatology shows that the Somali jet is the primary contributor of the moisture transport (+86.5 ms^{-1} gKg^{-1}) from the southern Indian Ocean into the Indian subcontinent across the west coast of Indian (+110.7 ms^{-1} gKg^{-1}), while moisture transport from the Atlantic Ocean across central Africa (+25.5 ms^{-1} gKg^{-1}) plays a secondary role in contributing a non-negligible amount , approximately 23%, to the total moisture flux into the Indian subcontinent. For EASM, which is downstream of the SASM, the moisture transport from the Indian Ocean and the tropical western Pacific across central East Asia (+41.0 ms^{-1} gKg^{-1}) to northeastern East Asia (+19.8 ms^{-1} gKg^{-1}) is much weaker compared to SASM. Under GHG, a large increase (8.8%) of moisture transport into SASM, with substantial contribution from both the Somali jet and Central Africa. Even though the climatology moisture flux in EASM is weaker than SASM, the relative impact of GHG, as measured by the percentage increase in moisture transport into East Asia, is stronger, with +18.2% across central East Asia and +11.7% across northern East Asia. Under ALL, all moisture fluxes remain positive*, i.e.,* enhanced relative to PI, but are significantly subdued compared to GHG. The inferred anthropogenic aerosol impact, IAA, portrays a strong negative anomalous moisture transport, *i.e.*, substantially less (relative to PI) moisture available for monsoon rainfall for both SASM and EASM. The IAA impact appears to be stronger for EASM compared to SASM, as evident in the larger percentage

reduction of moisture transport for EASM (-21.8% for central East Asia, and -14.9% for northeastern East Asia), compared to SASM (-7.1%).

a. Moist Static Stability (MSE)

To illustrate changes in the stability controls affecting the regional monsoons, anomalous MSE (= $C_pT + L_sq + gz$), where C_p is the heat capacity at constant pressure, L_s the latent heat of condensation, and z the geopotential height, has been computed for the SASM (70-100^{o}E) and EASM (100-130^{o}E) sectors, respectively. For SASM under GHG warming, the lower troposphere is conditionally unstable, as indicated by the vertical gradient of the MSE. The near surface MSE over SASM is strongly enhanced from the Indian Ocean and the Indian subcontinent, up to the southern slopes of the Tibetan Plateau (Fig.5a). Separate calculations (not shown) indicate that the increase in low-level MSE is due primarily to moisture effect (qL_s), although temperature effect (C_pT) also contributes. However, above 500 hPa, the gradient of the MSE (increasing with height) indicates increased atmospheric stability due mainly to moist adiabatic temperature effect from ascent of warmer air over a warmer surface. Above 200 hPa, convective instability is again enhanced. Notice that the mid- and upper troposphere over the Indian Ocean and southern land regions (10^{o}S-15^{o}N) is warmer than that over the monsoon land regions to the north. This is because of the much higher TPW over the large span of the warming Indian Ocean than over monsoon continental land, even though the latter is warmer than the former, *i.e.*, positive WOWL. Under GHG, ascending warm moist parcels over the Indian Ocean, by conservation of MSE, will convert more latent heat (moisture) to sensible heat (temperature) and thus causing the upper troposphere to warm faster and more over oceans than monsoon land to the north. Past studies (Li and Yanai, 1996, and others) have shown that a stronger SASM is

337 associated with positive upper tropospheric temperature gradient, *i.e.*, warmer north,
338 cooler south. Thus, under GHG, the tropospheric meridional temperature gradient actually
339 favors a *weaker* SASM monsoon, because the upper troposphere over the deep tropics is
340 warmer than over monsoon land, even though WOWL is positive at the surface (Fig. 1).
341 The IAA effect features a strong reduction in MSE near the surface and in the lower
342 troposphere over land (Fig. 5b). This is likely due to the reduced WOWL by strong cooling
343 of the land surface via the aerosol solar dimming effect, and the semi-direct effect in
344 increasing atmospheric stability in the lower troposphere (Allen and Sherwood, 2010).
345 For EASM (Fig. 5c and d), similar changes in MSE under GHG warming and by IAA
346 can be seen, reflecting competing stability controls within GHG, and between GHG and
347 aerosols, as in SASM. The main difference is that in EASM, under GHG, the region of
348 increased low-level MSE extends further poleward beyond 40^{o}N, due to the absence of
349 topographic blocking of moisture transport by the Tibetan Plateau. Under IAA (Fig. 5d)
350 the strongest impacts by aerosol, as reflected by the maximum reduction in low-level MSE,
351 is found near 35-50^{o}N, which collocates with the major industrial mega-metropolis of
352 central and northern East Asia, where aerosols emissions have been increasing steadily in
353 the last several decades (Liu et al., 2009). Note that the regional MSE anomalies are highly
354 consistent among models under GHG-only for both SASM and EASM (Fig. 5a, c), while
355 under All, the consistency is low (Fig. 5c, d), reflecting large uncertainty in aerosol physics
356 in the models.
357
358 *c. Changes in meridional circulation, rainfall, and atmospheric stability*

359 The climatology and anomalies of the monsoon meridional circulation (MMC) and
360 rainfall will be compared and contrasted for the SASM and EASM in this subsection. For
361 SASM, the climatological MMC comprises of strong rising motions from equator to the
362 Indian subcontinent characteristic by a sharp northern boundary demarked by strong
363 rising motion over the southern slope, and the top of Tibetan Plateau near 30-35^{o}N, and
364 weak sinking motion further north (Fig. 6a). Strong cross-equatorial flows in the upper
365 troposphere and near the surface connect the monsoon ascending to the descending
366 branch over 20-10^{o}S (Fig. 6a). Under GHG, increased WOWL effect drives strong low-level
367 moist transport from the ocean to the foothills of the Tibetan Plateau, increasing local MSE
368 near the surface and the lower troposphere (See discussions for Fig. 5). However, the
369 increase in local MSE does not give rise to an enhanced singular monsoonal large-scale
370 circulation, because of different stability controls in the lower to upper troposphere due to
371 local (moist adiabatic warming) and remote forcing, *i.e.*, DTS induced tropospheric RH
372 reduction and subsidence, on the Asian monsoon region. Strong sinking motion, driven by
373 the subsiding branch of the anomalous Walker Circulation prevails over 10^{o}S-10^{o}N (see
374 discussion in Section 3.2). Ascending motions north of 30^{o}N are capped to below 400 hPa.
375 Here, the growth of deep convection is inhibited because the rising moist air associated
376 with enhanced convection from the planetary boundary layer over northern Indian and the
377 Tibetan Plateau encounters large-scale subsidence and drier mid- troposphere air aloft,
378 leading to enhanced dry entrainment and suppression of deep convection and clouds (Del
379 Genio, 2012). As a result, deep convection arising from WOWL can only break out over
380 sub-domains of the SASM, *i.e.,* 15-25^{o}N, and 0-10^{o}N, where convective instability
381 overcomes atmospheric stability, giving rise to the appearance of multi-cell anomalous

382 MCC south of the Tibetan Plateau, and a relatively shallow circulation cell over and north
383 of the Tibetan Plateau (Fig. 6b). In contrast, IAA sustains a pronounced weakening SASM
384 MMC, in the form of a singular reversed monsoon cell with anomalous rising motion near
385 10^{o} S- equator, strong sink motion over the entire India subcontinent, and anomalous low
386 level moisture transport from *land to ocean* (Fig. 6c). Under GHG, rainfall is increased over
387 the entire SASM region (Fig. 6d), with maxima that match well with the regions of deep
388 ascent (Fig. 6b). Strong aerosol stabilizing effects negate all the rainfall increase due to
389 GHG, as evident in the systematically reduction of rainfall, over the entire SASM domain
390 under IAA (Fig. 6d)

391 For EASM, the climatological MMC (Fig. 6e) is similar to SASM, except with a less well-
392 defined northern boundary, characterized by gradually weakening rising motion up to
393 45^{o}N and beyond, due to the lack of topographic blocking by high mountains. Under GHG,
394 the MMC is dominated by strong anomalous subsidence over 10^{o}S- 0, due to the influence
395 of anomalous Walker Circulation. Elsewhere, anomalously weak subsidence prevails, in
396 spite of the strong transport moisture from ocean to land near the surface (Fig. 6f, see also
397 Fig. 6a). Here, deep convection and ascending motions are strongly inhibited by the
398 increase in atmospheric stability due to moist adiabatic effect, as well as the remotely
399 forced mid-tropospheric dryness over subtropical and extratropical land regions. Yet,
400 because of the pronounced increased in low-level MSE from increased moisture transport
401 associate with positive WOWL, rainfall is increased over the entire EASM domain (Fig. 7h).
402 The rainfall increase is most likely coming from shallow convection, and warm clouds. The
403 changing characteristics of monsoon rainfall under GHG and aerosol forcing is a subject of
404 an ongoing investigation to be reported in a forthcoming paper. As a result of the

405 increased stability at the mid-to-upper troposphere, GHG warming alone can have
406 competing regional effects that can lead to enhanced rainfall and a weakened MMC in
407 EASM. Under IAA, aerosols weakens the MMC substantially, as depicted by anomalous
408 overall sinking motion over all EASM land, and anomalous low-level moisture transport
409 from land to ocean, effectively drying out the EASM (Fig. 6g), and leading to overall
410 reduction in rainfall over EASM (Fig.6h).

411 Using Eq (1), we can estimate the changes in overall stability parameter M in relation
412 to changes in monsoon rainfall (P), and circulation (W) for SASM and EASM. As a proxy for
413 W, we use the vertical motion at 500 hPa. Table 3 shows the anomalies in P, W and M as
414 fractional changes relative to the PI climatology, averaged over the e SASM and EASM
415 sectors respectively. Briefly, under GHG, both monsoons show increasing rainfall coupled
416 to a weakening circulation. However, SASM has higher GHG rainfall sensitivity (+4.13%)
417 than EASM (+2.26%), but less circulation sensitivity (-1.34%) than EASM (-3.11%). The
418 overall change in M reflects approximately the same increase in convective stability
419 ($\Delta M/M>0$) for both monsoon, with +5.47% for SASM and +5.37% for EASM consistent with
420 the global scale nature of the GHG forcing. Under ALL, both SASM and EASM exhibit strong
421 aerosol effects in negating the GHG rainfall increase, and in further weakening of the
422 circulation through an increase in overall convective stability, *i.e.,* smaller values of positive
423 $\Delta M/M$ compared to GHG, for both monsoons. Specifically under ALL, aerosol effect leads to
424 rainfall reduction and circulation weakening at -5.59%, and -4.02% respectively for SASM,
425 compared to EASM at -6.01%, and -3.32% respectively. As shown in IAA, anthropogenic
426 aerosols exert stronger stabilizing effect, *i.e.*, more negative $\Delta M/M$, for EASM (-2.69%)
427 compared to SASM (1.57%). These similarities and contrasts in sensitivities of rainfall,

circulation and convective stability between SASM and EASM are likely to stem from the differences in climatological mean states, regional feedback processes, which are dependent on different land-sea configuration, topographic influences, and aerosol types, *e.g*., absorbing v. scattering aerosols, in these two regional monsoons (Li et al., 2016).

d. Observed rainfall comparison

In this subsection, we provide an assessment of the realism of the MMM rainfall anomalies from GHG and ALL experiments, in comparison with observed rainfall trend derived from 36 years of rainfall observations from APHRODITE (Yatagai et al., 2012), which provides daily gridded rainfall at 0.25 x0.25 resolution over the greater Asian monsoon land domain including Middle East, and northern Eurasia for 57 years (1961-2007). Under GHG, the MMM rainfall anomaly pattern (Fig. 7a) shows increased rainfall over two key regions: 1) the Indian subcontinent, the Tibetan Plateau, and adjacent oceans including the Bay of Bengal, southern Arabia Sea, and the equatorial Indian Ocean, and 2) the western tropical Pacific and northern Pacific over northeastern China, Korea and Japan. Rainfall increase is weak between 100-120^{o} E, possibly due to the strong influence of mid-tropospheric dryness and subsidence induced by DTS, in connection with a weakening of Walker circulation under GHG warming (Fig. 3). It is also noted that the consistency (> 75% of models agree in the sign of the anomaly) among CMIP5 models is quite high in regions where the rainfall is substantially increased. Under ALL, the aerosol effect essentially overwhelms the GHG effect, resulting in reduced precipitation over most the Asian regions, in a pattern resembling a “dry land arc” following the continental outline of the Asian land mass from Northeastern China, Japan and Korean, through central and eastern China, Southeast Asia, eastern India to the

Maritime continent, and adjacent oceans. What appears to be remnant of increased rainfall due to GHG warming is only found over the tropical western Pacific. Anthropogenic aerosol effects, as reflected in IAA (Fig. 7c), cause dominant reduction in rainfall over the entire monsoon land and ocean regions. Noting that there are only few regions in which the CMIP5 models meets the 75% consistency test (Fig. 7b), the reliability of the results for ALL and for IAA is likely to be much lower than that for GHG.

There are similarities between ALL (Fig.7b) and observed rainfall (Fig. 7d), specifically in the "dry land arc" from northeastern China, through India, Southeast Asia, to the Maritime continent. However, regional details are not well matched between ALL and observation. In ALL, the MMM rainfall anomaly fails to reproduce the increased rainfall over central and southern China - a component of the well-known NDSW observed pattern of the EASM. Over India, pockets of increased rainfall over northeastern and northwestern coastal regions are not simulated. However, as indicated by the scarcity of regions demonstrating model consistency, the ALL and IAA results may be subject to larger model diversities and uncertainties compared to GHG. Given the large inconsistency among model rainfall simulations under ALL, it is possibly that model may have been overly sensitive to aerosols forcing (Anderson et al., 2003; Kiehl, 2007). Because of strong dynamical feedback in the monsoon ocean-land-atmosphere system, a slightly larger aerosol forcing over GHG effect could be amplified, through global-scale coupled ocean-atmosphere-land feedback, into strong negative IAA rainfall anomalies over the entire region.

4. Conclusions

We have carried out an analysis of changes and impacts of key global and regional drivers for GHG warming and aerosols on the circulation and rainfall of the SASM and EASM respectively, based on CMIP5 historical simulations during the boreal summer season, JJA. Results show large competing influences in monsoon driver and responses within GHG warming alone, and between GHG and aerosol forcing and responses, in effecting changes in rainfall and circulation in Asian monsoon regions. Key findings include:

- GHG forcing induces a strong warm-ocean-warmer-land (WOWL) effect, significantly enhancing the thermal contrast between global land and ocean, and between the NH and SH in the last 5 decades, since 1950. The WOWL effect is responsible for increased moisture transport from ocean to land over monsoon region, but is strongly masked by aerosols, up to 60% in NH monsoon land and ocean regions in recent decades.
- GHG forcing induces a global drying (reduction of relative humidity) tendency in the mid- to-lower troposphere and near the land surface of the NH subtropics and extratropics, in conjunction with the development of the Deep Tropical Squeeze (DTS) - a tightening of the ascending branch of Hadley Circulation coupled to a widening of the subsidence regions (Lau and Kim, 2015b). Anomalous subsidence is also found over the oceanic, and southern land regions of the Asian monsoon associated with a weakening of the Walker Circulation under global warming. The large-scale subsidence and tropospheric relative humidity reduction, exert strong negative impacts *i.e.,* suppressing

rainfall, and weakening circulation, particularly over the Asian monsoon land regions.

- Aerosols strongly mask the GHG WOWL effect, over 60% in the NH, thereby weakening the DTS, and associated negative remote forcing of the Asian monsoon. However, aerosol induced local stability via solar dimming and semi-direct effects, strongly weakens the monsoon large-scale circulation, negating to a large extent the tendency to increase rainfall from GHG warming.
- Both SASM and EASM are sensitive to anthropogenic aerosol forcing, with strong reduction in rainfall and weakening of the monsoon circulation. SASM is more sensitive to GHG warming in terms of enhancing rainfall, and EASM more sensitive to GHG stability effect in terms of circulation weakening.

It is important to note that above findings are all based on CMIP5 historical simulations, and relevant for anomalies of recent decades, compared to the pre-industrial control. The results are only trustworthy to the extent that the MMM quantities are good proxies of the real world. Comparison between ALL rainfall anomaly and APHRODITE observed rainfall trend pattern does not show a good match over the Asian monsoon region. The largest discrepancy is in the increased rainfall over central and southern China*, i.e.*, the southern portion of the North-Dry-South-Wet long-term rainfall pattern over East Asia, which are missing in the MMM. Yet, both ALL and observation, but not GHG-only, show a "dry land arc" spanning northeastern Asia, western China, Indo-China and the Maritime Continent, hinting at a possible aerosol induced large-scale footprint on Asian monsoon rainfall. Because there is no real world observation for GHG-only forcing and response, validation is impossible. However, based on model consistency (Fig.

522 7a), the reliability of results for GHG-Only is substantially higher than the ALL
523 experiments, in agreement with previous studies (Ma et al., 2016) This is also consistent
524 with the fact that aerosol and clouds are still the two largest sources of uncertainties in
525 CMIP5 climate models. There are other fundamental reasons why the modeled MMM
526 rainfall anomalies do not match well with observations. First among them are inadequate
527 model physics, and coarse model resolution that are incapable of simulating detailed
528 rainfall and aerosol processes, particular with respect to aerosol-cloud-monsoon
529 dynamics interactions. Another is that MMM is a measure of the forced response to
530 imposed externally prescribed emission forcing with model internal variability minimized,
531 while observations represents a singular and imperfect realization of the real world for
532 the last several decades. The observed trend is likely to be reflected as a mix of forced
533 responses and natural variability including secular long-term variations, and multi-
534 decadal oscillations that have been shown to influence long-term rainfall changes over the
535 Asian monsoon region (Wang et al., 2013; Krishnamurthy and Krishnamrthy, 2014, and
536 many others). Our results suggest that, consistent with changes in fundamental
537 thermodynamics (temperature, moist static energy) and dynamic (circulation) controls of
538 the Asian monsoon, there are some degree of similarity between ALL and the observed
539 rainfall trends over monsoon land. This means that in recent decades, and possibly in the
540 near future, there may be emerging broad scale signals of anthropogenic forcing and
541 responses in different regions of Asian monsoon, attributable respectively to GHG,
542 aerosols or combined effects, based on physical rather than strictly statistically
543 considerations. This work represents a modest first step towards establishing a baseline

for a holistic understanding Asian monsoon regional climate change under GHG and aerosol forcing.

While our results show that the global and large-scale forcing, *i.e.*, the WOWL effect, hemispheric thermal asymmetry, mid-tropospheric dryness, moisture transport and moist static energy, affect the Asian monsoon as a whole, the component monsoon forcing and responses , i.e., SASM vs. EASM, could be quite different because of regional feedback processes involving interactions of monsoon dynamics and aerosols, both natural and anthropogenic, modulated by regional land-sea configuration, and orography. These interactions occur on diverse spatio-temporal scales from individual clouds (~hours) to climate change (>100 years) and beyond (Lau, 2014, 2016). Therefore, it is important that for future work, model experiments and observational analysis should also be carried out not only for monsoon climate change, but also on intraseasonal and interannual variability in order to provide better understanding of aerosol dynamical feedback such as the Elevated Heat Pump (EHP) effects and related processes (Vinoj et al., 2014, Jin et al., 2014, Fan et al. 2015, Kim et al., 2015, Lau et al., 2016). Even under the current fast pace of industrialization, natural aerosols (desert dust, black carbon and organic carbon from wildfires, and sulfates from volcanic eruptions) are still several times more abundant than anthropogenic aerosols in the Asian monsoon regions (Satheesh and Moorthy, 2005). They are likely to play an important role in modulating intrinsic monsoon processes such as onset, breaks and extreme heavy rain events, as well as climate change.

Acknowledgement This work is partially supported by the Department of Energy/ Pacific Northwest National Laboratory Grant 4313671 to ESSIC, University of Maryland, and the NASA Modeling, Analysis and Prediction (MAP) Program.

Reference

Allen, R. J., and S. C. Sherwood, 2010: Aerosol-cloud semi-direct effect and land-sea temperature contrast in a GCM. *Geophys. Res. Lett.*, **37**, L07702, doi:10.1029/2010GL042759.

Anderson A., R. Charlson, S. Schwartz, R. Knutti, O. Boucher, H. Rodhe, and J. Heintzenberg, 2003: Climate Forcing by Aerosols - a Hazy Picture. *Science,* **300**, 1103-1104 DOI: 10.1126/science.1084777

Annamalai, H., J. Hafner, K. P. Sooraj, and P. Pillai, 2013: Global warming shifts the monsoon circulation, drying South Asia. *J. Climate*, **26**, 2701-2718.

Bollasina, M. A., Y. Ming, V. Ramaswamy, M. D. Schwarzkopf, and V. Naik, 2014: Contribution of local and remote anthropogenic aerosols to the twentieth century weakening of the South Asian Monsoon. *Geophys. Res. Lett.,* **41**, 680–687, doi:10.1002/2013GL058183.

Bollasina, M., Y. Ming, and V. Ramaswamy, 2011: Anthropogenic aerosols and the weakening of the South Asian summer monsoon. *Science*, **334**, doi:10.1126/science.1204994

588 Cheng, Q., and T. Zhou, 2014: Multidecadal Variability of North China Aridity and Its
589 Relationship to PDO during 1900–2010. *J. Climate,* **27**, 1210–1222, doi:
590 10.1175/JCLI-D-13-00235.1.
591 Chung, C. E., and V. Ramanathan, 2006: Weakening of north Indian SST gradients and the
592 monsoon rainfall in India and the Sahel. *J. Climate*, **19**, 2036-2045.
593 Cowan, T., and W. Cai, 2011: The impact of Asian and non-Asian anthropogenic aerosols on
594 20th century Asian summer monsoon. *Geophys. Res. Lett.,* **38**, L11703,
595 doi:10.1029/2011GL047268.
596 Dai, A., 2011: Drought under global warming: A review. WIREs *Climate Change,* **2**, 45–65.
597 Dai, A., 2006: Recent climatology, variability and tends in global surface humidity. *J.*
598 *Climate*, **19**, 3589-3606.
599 Del Genio, A.D., 2012: Representing the Sensitivity of Convective Cloud Systems to
600 Tropospheric Humidity in General Circulation Models. *Surv. Geophys.* **33**, 637-
601 656, doi:10.1007/s10712-011-9148-9
602 Dickinson, R.E., Meehl, G.A., and Washington, W.M., 1987: Ice-albedo feedback in a CO_2-
603 doubling simulation , *Climatic Chan*ge, **10**, 241-248, doi:10.1007/BF00143904
604 Ding, Y., Wang, Z., and Sun, Y., 2008: Inter-decadal variation of the summer precipitation in
605 East China and its association with decreasing Asian summer monsoon. Part I:
606 Observed evidences. *Int. J. Climatol*., **28**, 1139–1161, doi:10.1002/joc.1615
607 Fan, J., L. R. Leung, D. Rosenfeld, Q. Chen, Z. Li, J. Zhang, and H. Yan , 2013: Microphysical
608 effects determine macrophysical response for aerosol impacts on deep convective
609 clouds. *Proc. Natl. Acad. Sci. U. S. A.*, **110**, E4581–90,
610 doi:10.1073/pnas.1316830110.

611 Fan, J. W., D. Rosenfeld, Y. Yang, et al., 2015: Substantial contribution of anthropogenic air
612 pollution to catastrophic floods in Southwest China. Geophys. Res. Lett., **42**, 6066–
613 6075, doi:0.1002/2015GL064479.
614 Fu, Q., and Feng, S., 2014: Responses of terrestrial aridity to global warming. *J. Geophys.*
615 *Res*., **119**, doi:10.1002/2014JD021608.
616 Ganguly, D., P. J. Rasch, H. Wang, and J.-H. Yoon, 2012: Climate response of the South Asian
617 monsoon system to anthropogenic aerosols. *J. Geophys. Res.,* **117**, D13209,
618 doi:10.1029/2012JD017508.
619 Holton, J. R., 1992: *An Introduction to Dynamic Meteorology*, 3rd Edition, Academic Press
620 Inc., ISBN 012-354355-X.
621 IPCC, 2013: *Climate Change 2013: The Physical Science Basis, the contribution of Working*
622 *Group I to the Fifth Assessment Report of the Intergovernmental Panel on Climate*
623 *Change*, edited by Stocker, T.F., D. Qin, G.-K. Plattner, M. Tignor, S.K. Allen, J.
624 Boschung, A. Nauels, Y. Xia, V. Bex and P.M. Midgley, Cambridge University Press,
625 Cambridge, UK and New York, NY, USA.
626 Jin, Q., J. Wei*, and* Z.-L. Yang *(*2014*),* Positive response of Indian summer rainfall to Middle
627 East dust*, Geophys. Res. Lett.,* 41*,* 4068–4074*, doi:*10.1002/2014GL059980
628 Kim, M. K., W. K. M. Lau, K-M. Kim, J. Sang, Y-H Kim and W-S Lee (2015), Amplification of
629 ENSO effects on Indian summer monsoon by absorbing aerosols, *Clim. Dyn*., DOI
630 10.1007/s00382-015-2722-y
631 Kiehl, J. T., 2007: Twentieth century climate model response and climate
632 sensitivity. *Geophys. Res. Lett*., **34**, L22710, doi:10.1029/2007GL031383.

633 Krishnamurthy, L., and V. Krishnamurthy, 2014: Decadal scale oscillations and trend in
634 the Indian monsoon rainfall. *Clim Dyn,* **43**: 319-331, doi:10.1007/s00382-013-
635 1870-1
636 Lau, W. K. M., 2014: Desert Dust and Monsoon Rainfall, *Nature, Geoscience, 7, 255-256,*
637 doi:10.1038/ngeo2115
638 Lau, W. K. M., 2016: The aerosol-monsoon climate system of Asia: A new paradigm, *J.*
639 *Meteorol. Res*., 29(6), 1–11, doi:10.1007/s13351-015-5999-1.
640 Lau, K. M., and M. T Li, 1984: The Monsoon of East-Asia - A Survey. *Bull. Amer*. *Meteor. Soc*.,
641 **65**, 114-125.
642 Lau, K. M., and K. M. Kim, 2006: Observational relationships between aerosol and Asian
643 monsoon rainfall, and circulation, *Geophys. Res. Lett*., **33**, L21810,
644 doi:10.1029/2006GL027546.
645 Lau, W. K.M., and K. M. Kim, 2010: Fingerprinting the impacts of aerosols on long-term trends
646 of the Indian summer monsoon regional rainfall. *Geophys. Res. Lett*, **37,** L16705,
647 doi:10.1029/2010GL043255.
648 Lau, K. M., M. K. Kim, and K. M. Kim, 2006: Asian summer monsoon anomalies induced by
649 aerosol direct forcing: the role of the Tibetan Plateau. *Clim. Dyn.*, **26**,
650 doi:10.1007/s00382-006-0114-z.
651 Lau, W. K. M., H. T. Wu, and K-M Kim, 2013: A canonical response in rainfall characteristics
652 to global warming from CMIP5 model projections. *Geophys. Res. Lett*. 40,
653 doi:10.1002/grl.50420.
654 Lau, K.M., V. Ramanathan, G-X. Wu, Z. Li, S. C. Tsay, C. Hsu, R.Sikka, B. Holben, D. Lu, G.
655 Tartari, M. Chin, P .Koudelova, H. Chen, Y. Ma, J. Huang, K. Taniguchi, and R. Zhang ,

2008: The Joint Aerosol-Monsoon Experiment: A New Challenge in Monsoon Climate Research. *Bull. Am. Meteor. Soc*., **89**, 369-383, DOI:10.1175/BAMS-89-3-369.

Lau, K. M., and K.M. Kim, 2015a: Impacts of absorbing aerosols on the Asian monsoon: An Interim Assessment. In, *World Sci. Series on Asian-Pacific Weather and Climate, Vol. 6, Climate Change: Decadal and Beyond,* Ed: C. P. Chang, M. Ghil, M. Latif, and J. M. Wallace.

Lau, W. K. M., and K. M. Kim, 2015b: Robust responses of the Hadley circulation and global dryness form CMIP5 model CO_2 warming projections. *Proc. Natl. Acad. Sci.,* **112**, 3630-3635, doi: 10.1073/pnas.1418682112.

Lau, W. K. M., K. M., Kim, J.J., Shi, T. Matsui, M. Chin, Q. Tan, C. Peters-Lidard, W. K. Tao, 2016: Impacts of aerosol–monsoon interaction on rainfall and circulation over Northern India and the Himalaya Foothills. *Clim. Dym,* doi: 0.1007/s00382-016-3430-y

Lee, J., and B. Wang, 2014: Wang, Future change of global monsoon in the CMIP5. *Clim Dyn,* **42**: 101-119, doi:10.1007/s00382-012-1564-0.

Li, C., and M. Yanai, 1996: The Onset and Interannual Variability of the Asian Summer Monsoon in Relation to Land–Sea Thermal Contrast. *J. Climate,* **9**, 358–375.

Li, X., M. Ting, C. Li, and N. Henderson (2015), Mechanisms of Asian summer monsoon changes in response to anthropogenic forcing in CMIP5 models, *J. Climate*, 28, 4107–4125.

Li, Z., W.K.-M. Lau, V. Ramanathan, G. Wu, Y. Ding, M.G. Manoj, Y. Qian, J. Li, T. Zhou, J. Fan, D. Rosenfeld, Y. Ming, Y. Wang, J. Huang, B. Wang, X. Xu, S.-S., Lee, T. Takemura, K.

679 Wang, X. Xia, Y. Yin, H. Zhang, J. Guo, N. Sugimoto, J. Liu, and X. Yang, 2016: Aerosol
680 and monsoon climate interactions over Asia. *Review of Geophys.* 54, doi:10.1002/
681 2015RG000500
682 Liu, Y., J. Sun, and B. Yang, 2009: The effects of black carbon and sulphate aerosols in China
683 regions on East Asia monsoons, *Tellus, Ser. B Chem. Phys. Meteorol.*, **61**, 642-656,
684 doi:10.1111/j.1600-0889.2009.00427.x.
685 Man, W. T. Zhou, J. H. Jungclaus, 2014: Effects of large volcanic eruption on global
686 summer climate and East Asian monsoon changes during the last millenium:
687 Analysis of MPI-ESM simulations. *J. Climate*, 27, 7394-7409.
688 Meehl, G., J. Arblaster, and W. Collins, 2008: Effects of black carbon aerosols on the Indian
689 monsoon, *J. Climate*, **21**, 2869-2882, doi:10.1175/2007JCLI1777.1.
690 Menon, S., J. Hansen, L. Nazarenko, and Y. Luo, 2002: Climate effects of black carbon
691 aerosols in China and India, *Science*, **297** (5590), 2250-2253,
692 doi:10.1126/science.1075159.
693 Polson, D., M. Bollasina, G. C. Hegerl, and L. J. Wilcox, 2014: Decreased monsoon
694 precipitation in the Northern Hemisphere due to anthropogenic aerosols. *Geophys.*
695 *Res. Lett.*, **41**,6023-6029, doi:10.1002/2014GL060811.
696 Ramanathan, V., and G. Carmichael, 2008: Global and regional climate changes due to black
697 carbon, *Nat. Geosci*., **1**, 221-227, doi:10.1038/ngeo156.
698 Ramanathan, V., and Y. Feng, 2009: Air pollution, greenhouse gases and climate change:
699 Global and regional perspectives. *Atmos. Environ*., **43**, 37-50,
700 doi:10.1016/j.atmosenv.2008.09.063.

701 Randles, C. A., and V. Ramaswamy, 2008: Absorbing aerosols over Asia: A Geophysical
702 Fluid Dynamics Laboratory general circulation model sensitivity study of model
703 response to aerosol optical depth and aerosol absorption, *J. Geophys. Res.*, **113**,
704 D21203, doi:10.1029/2008JD010140.
705 Robock, A., 2000: Volcanic eruptions and climate, *Rev. Geophys.*, **38**(2), 191–219,
706 doi:10.1029/1998RG000054.
707 Rosenfeld, D., U. Lohmann, G. B. Raga, C. D. O'Dowd, M. Kulmala, S. Fuzzi, A. Reissell, and M.
708 O. Andreae, 2008: Flood or drought: how do aerosols affect precipitation? *Science*,
709 **321**, 1309-1313, doi:10.1126/science.1160606.
710 Roxy, M. K., K. Ritika, P. Terray, R. Murtugudde, K. Ashok, and B. Goswami, 2015: Drying of
711 Indian subcontinent by rapid Indian Ocean warming and a weakening land-sea
712 thermal gradient. *Nature Communications*, **6**, 7423, doi:10.1038/ncomms8423.
713 Santers et al. 2013, Identifying human influences on atmospheric temperature. *Proc. Natl.*
714 *Acad. Sci.,* **110** (1) 26-33; doi:10.1073/pnas.1210514109.
715 Satheesh S. K., and K. K. Moorthy, 2005: Radiative effects of natural aerosols: A
716 review. *Atmos. Environ*. 39, 2089–2110, doi: 10.1016/j.atmosenv.
717 2004.12.029.
718 Sherwood, S. C., W. Ingram, Y. Tsushima, M. Satoh, M. Roberts, P. L. Vidale, and P. A.
719 O'Gorman, 2010: Relative humidity changes in a warmer climate. *J. Geophys. Res.*,
720 **115**, D09104, doi:10.1029/2009JD012585.
721 Song, F., T. Zhou, and Y. Qian, 2014: Responses of East Asian summer monsoon to natural
722 and anthropogenic forcings in the 17 latest CMIP5 models. *Geophys. Res. Lett.*, **41**,
723 596-603, doi:10.1002/2013GL058705.

724 Tokinaga, H, S. P. Xie, and A. Timmermann, 2012: Regional Patterns of Tropical Indo-
725 Pacific Climate Change: Evidence of the Walker Circulation Weakening. *J. Climate*,
726 **2**5, 1689- 1709, DOI: 10.1175/JCLI-D-11-00263.1.
727 Turner, A. G., and H. Annamalai, 2012: Climate change and the South Asian summer
728 monsoon. *Nature Climate Change*, **2**, 587-595, doi: 10.1038/NCLIMATE1495.
729 Vecchi, G. A., and B. J. Soden, 2007: Global Warming and the Weakening of the Tropical
730 Circulation. *J. Climate,* **20**, 4316–4340, doi: 10.1175/JCLI4258.1.
731 Vinoj, V., P. J. Rasch, H. Wang, J.-H. Yoon, P.-L. Ma, K. Landu, and B. Singh, 2014: Short-
732 term modulation of Indian summer monsoon rainfall by West Asian dust. *Nat. Geosci.*,
733 **7**, 308–314, doi:10.1038/ngeo2107
734 Wang, B. J. Liu, H. Kim, P. Webster P., and S. Yim, 2012: Recent change of the global
735 monsoon precipitation (1979–2008). *Clim Dyn,* **39**, 1123–1135.
736 Wang, C., D. Kim, A. M. L. Ekman, M. C. Barth, and P. J. Rasch, 2009: Impact of
737 anthropogenic aerosols on Indian summer monsoon. *Geophys. Res. Lett.*, **36**,
738 L21704, doi:10.1029/2009GL040114.
739 Wang, B., J. Liu, H. Kim, P. J. Webters, S-Y. Yim, and B. Xiang, 2013a: Northern Hemisphere
740 summer monsoon intensified by mega-El Niño/southern oscillation and Atlantic
741 multidecadal oscillation. *Proc. Natl. Acad. Sci.*, **110**,. 5347-5352,
742 doi:10.1073/pnas.1219405110.
743 Wang, T., H. J. Wang, O. H. Otterå, Y. Q. Gao, L. L. Suo, T. Furevik, and L. Yu, 2013b:
744 Anthropogenic agent implicated as a prime driver of shift in precipitation in
745 eastern China in the late 1970s. *Atmos. Chem. Phys.*, **13**, 12433–12450.

746 Webster, P. J., V. O. Magaña, T. N. Palmer, J. Shukla, R. A. Tomas, M. Yanai, and T.
747 Yasunari, 1998: Monsoons: Processes, predictability, and the prospects for
748 prediction, *J. Geophys. Res.*, **103**(C7), 14451–14510,
749 doi:10.1029/97JC02719.
750 Yatagai, A., K. Kamiguchi, O.Arakawa, A. Hamada, N. Yasutomi, and A. Kitoh,
751 2012: APHRODITE: Constructing a Long-Term Daily Gridded Precipitation Dataset
752 for Asia Based on a Dense Network of Rain Gauges. *Bull. Amer. Meteor.*
753 *Soc.,* **93**, 1401–1415, doi: 10.1175/BAMS-D-11-00122.1.
754 Ye, J., W. Li, L. Li, and F. Zhang, 2013: "North drying and south wetting" summer
755 precipitation trend over China and its potential linkage with aerosol loading, *Atmos.*
756 *Res.*, **125-126**, doi:10.1016/j.atmosres.2013.01.007.
757 Yu, R., B. Wang and T. Zhou, 2004: Tropospheric cooling and summer monsoon
758 weakening trend over East Asia. *Geophys. Res. Lett.*, 31,L22212,
759 doi:10.1029/2004GL021270.
760 Yu, R., and T. Zhou, 2007: Seasonality and three dimensional structure of the interdecadal
761 change in East Asian monsoon. *J. Climate*, 20, 5344-5355.
762 Zhang, H., Z. Wang, P. Guo, and Z. Wang, 2009: A modeling study of the effects of direct
763 radiative forcing due to carbonaceous aerosol on the climate in East Asia. *Adv.*
764 *Atmos. Sci.*, **26**, 57-66, doi:10.1007/s00376-009-0057-5.
765 Zhang, L., and T. Li (2016), Relative roles of anthropogenic aerosols and greenhouse gases in
766 land and oceanic monsoon changes during past 156 years in CMIP5 models, *Geophys.*
767 *Res. Lett.*, *43*, 5295–5301.

768 Zhou, T., D. Gong, J. Li and B. Li, 2009: Detecting and understanding the multi-decadal
769 variability of the East Asian Summer Monsoon: Recent progress and state of affairs.
770 *Meteorologische Zeitschrift,* 18(4), 455-467
771 Zhou, T.,R. Yu, H. Li, and B. Wang, 2008: Ocean Forcing to Changes in Global Monsoon
772 Precipitation over the Recent Half-Century. *J. Climate,* **21**, 3833–3852, doi:
773 10.1175/2008JCLI2067.1.
774

775

776 Table 1 Anomaly (^{o}C) in MMM surface temperature (T_s) in last 25 year (1991-2005) of
777 model integration compared to climatology of pre-industrial period, computed for land
778 and ocean separately, and averaged over the globe, Northern Hemisphere and Southern
779 Hemisphere for GHG-only and ALL experiments respectively. The aerosol masking
780 effect is defined by $AME = 1 - \frac{\Delta T_{s,ALL}}{\Delta T_{s,GHG}}$.

781

	Global		NH		SH	
	Land	Ocean	Land	Ocean	Land	Ocean
GHG	1.39±0.17	0.81±0.15	1.49±0.23	0.93±0.12	1.18±0.26	0.72±0.21
ALL	0.59±0.12	0.41±0.14	0.57±0.19	0.35±0.11	0.65±0.26	0.46±0.21
AME	0.58	0.49	0.62	0.62	0.45	0.36

782
783
784
785
786
787
788
789
790

791 Table 2 850hPa moisture flux across key cross-sections affecting the SASM (West coast
792 of India) and EASM (Central East Asia, and Northeastern Asia), for GHG-only, ALL and
793 IAA respectively. See Fig. 4 for geographic locations of cross-sections.

794

Moisture Flux (m/s g/Kg)	Mean (PI)	GHG	ALL	IAA
Central Africa	25.5	5.5 (21.5%)	2.1 (8.2%)	-3.3 (-12.7%)
Somali Jet, Equator	86.5	12.3 (14.2%)	7.7 (8.9%)	-8.6 (-9.9%)
West coast of India	110.7	9.7 (8.8%)	1.1 (1.0%)	-7.9 (-7.1%)
Central East Asia	40.9	7.4 (18.2%)	2.0 (4.9%)	-8.9 (-21.8%)
Northeastern Asia	19.8	2.3 (11.7%)	0.7 (3.3%)	-2.9 (-14.9%)

795
796

797

798

799

800 Table 3 Percentage changes of precipitation ΔP/P, meridional circulation ΔW/W (W=

801 mean vertical motion at 500 hPa), and convective instability ΔM/M (=ΔP/P - ΔW/W),

802 averaged over the monsoon domain for SASM and EASM, as well as for GHG, ALL and

803 IAA respectively. Changes are relative to the pre-industrial climatology.

W500>0.0	SASM (70E-100E, 5N-30N)			EASM (100E-130E, 20N-45N)		
	ΔP/P	ΔW/W	ΔM/M	ΔP/P	ΔW/W	ΔM/M
GHG	4.13	-1.34	5.47	2.26	-3.11	5.37
ALL	-2.29	-5.38	3.09	-4.25	-5.94	1.69
IAA	-5.59	-4.02	-1.57	-6.01	-3.32	-2.69

804

805

806

807

808

Figure Captions

Figure 1 Spatial distribution of June-July-August MMM surface temperature anomalies (^{o}C) for GHG (a), and ALL (b), and time series of warm-ocean-warmer-land (WOWL) index (see text for definition) for ALL, GHG, Nat, and inferred anthropogenic aerosol effects , IAA = ALL-(GHG+Nat), and pre-industrial (PI) control respectively (c). Grid points where more than 75% (15 out of 19), and 65% (13 out of 19), of the percentage of ensemble members having the same sign as the MMM anomalies are indicted by black, and open circles, respectively.

Figure 2 June-July-August latitude-height profiles of zonally averaged climatological mean (contour) and anomalous (color) relative humidity (RH) in percentage for a) GHG, and b) ALL. Grid points where more than 75% (65%) of ensemble members have the same sign as the MMM anomalies are indicated by black (open) circles.

Figure 3 Left panels showing spatial distributions of RH anomalies at a) 500 hPa, b) 850 hPa, c) SST anomaly (^{o}C), and d) negative anomalous vertical p-velocity (10^{-2}hPa s^{-1}) for GHG, with contour showing climatology. Right panels, e), f), g) and h) are the same as corresponding left panels, except for ALL. Green dots in a), b), e) and f) denote regions of anomalous descent.

Figure 4 Spatial distribution of anomalous moisture transport (ms^{-1} gKg^{-1}) and 25-year (1981-2005) mean distribution of total precipitable water (g Kg^{-1}) for a) GHG and b) ALL. Key cross-sections for transport of moisture to SASM and EASM are shown in a).

832 Figure 5 MMM Moist Static Energy (MSE) anomalies for the SASM for a) GHG and b)
833 IAA, and same for c) and d), except for EASM. Units in kJ/Kg. Grid points
834 with black (open) circles indicate where more than 75% (65%) of the
835 ensemble members having the same sign as the MMM anomaly.
836 Figure 6 Left panels show spatial distribution and magnitude of June-July-August
837 vertical velocity (hPa s^{-1}) associated with the monsoon meridional
838 circulation of the SASM, for a) PI climatology, b) GHG induced anomalies, c)
839 IAA induced anomalies, and d) and rainfall anomalies due to GHG (red) and
840 due to IAA (blue), with error bars indicating model spread. Right panels e),
841 f), g) and h) are the same as corresponding left panels, except for the EASM.
842 Figure 7 Spatial distribution of June-July-August MMM rainfall anomalies (mm) for
843 a) GHG, b) ALL, c) IAA, and d) trends (mm $decade^{-1}$) during 1961-2007 from
844 APHRODITE rainfall observations. In a) and b), grid points in which more
845 than 75% of ensemble members having the same sign as the MMM anomalies
846 are indicated by green solid (open) circles.

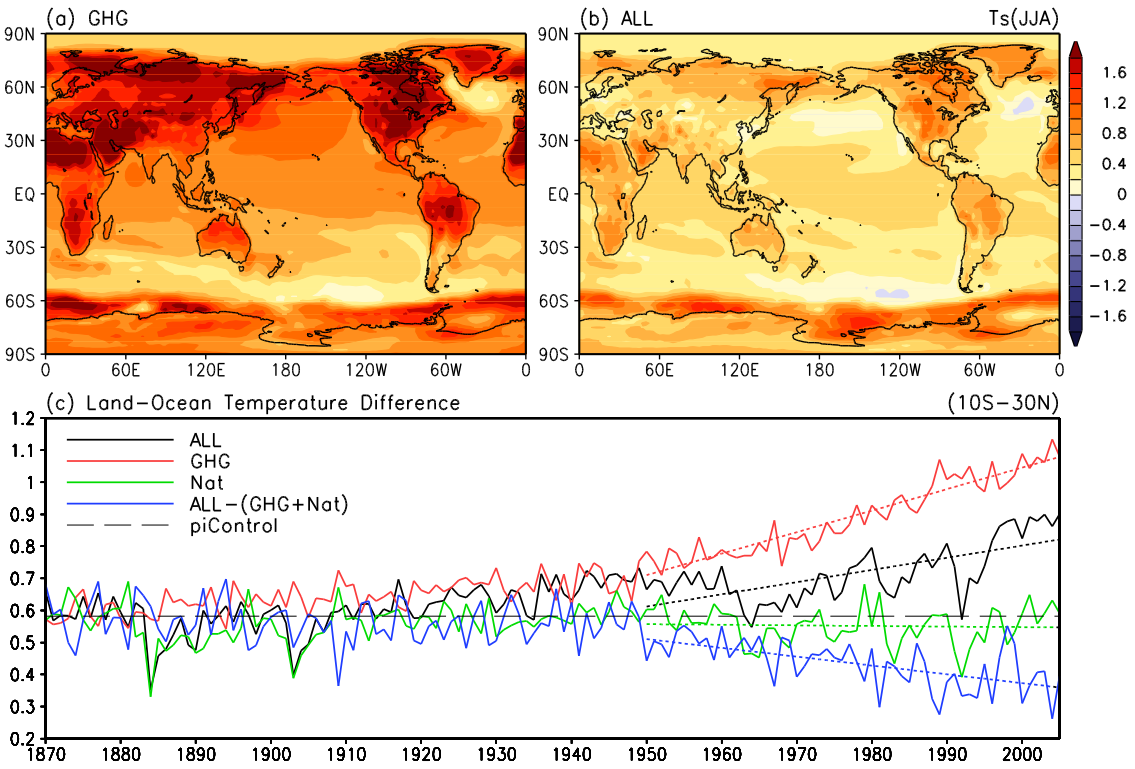
(a) GHG
(b) ALL
Ts(JJA)
90N
60N
30N
EQ
30S
60S
90S
0
60E
120E
180
120W
60W
1.6
1.2
0.8
0.4
0
−0.4
−0.8
−1.2
−1.6
(c) Land−Ocean Temperature Difference
(10S−30N)
ALL
GHG
Nat
ALL−(GHG+Nat)
piControl
1.2
1.1
1
0.9
0.8
0.7
0.6
0.5
0.4
0.3
0.2
1870
1880
1890
1900
1910
1920
1930
1940
1950
1960
1970
1980
1990
2000

Figure 1

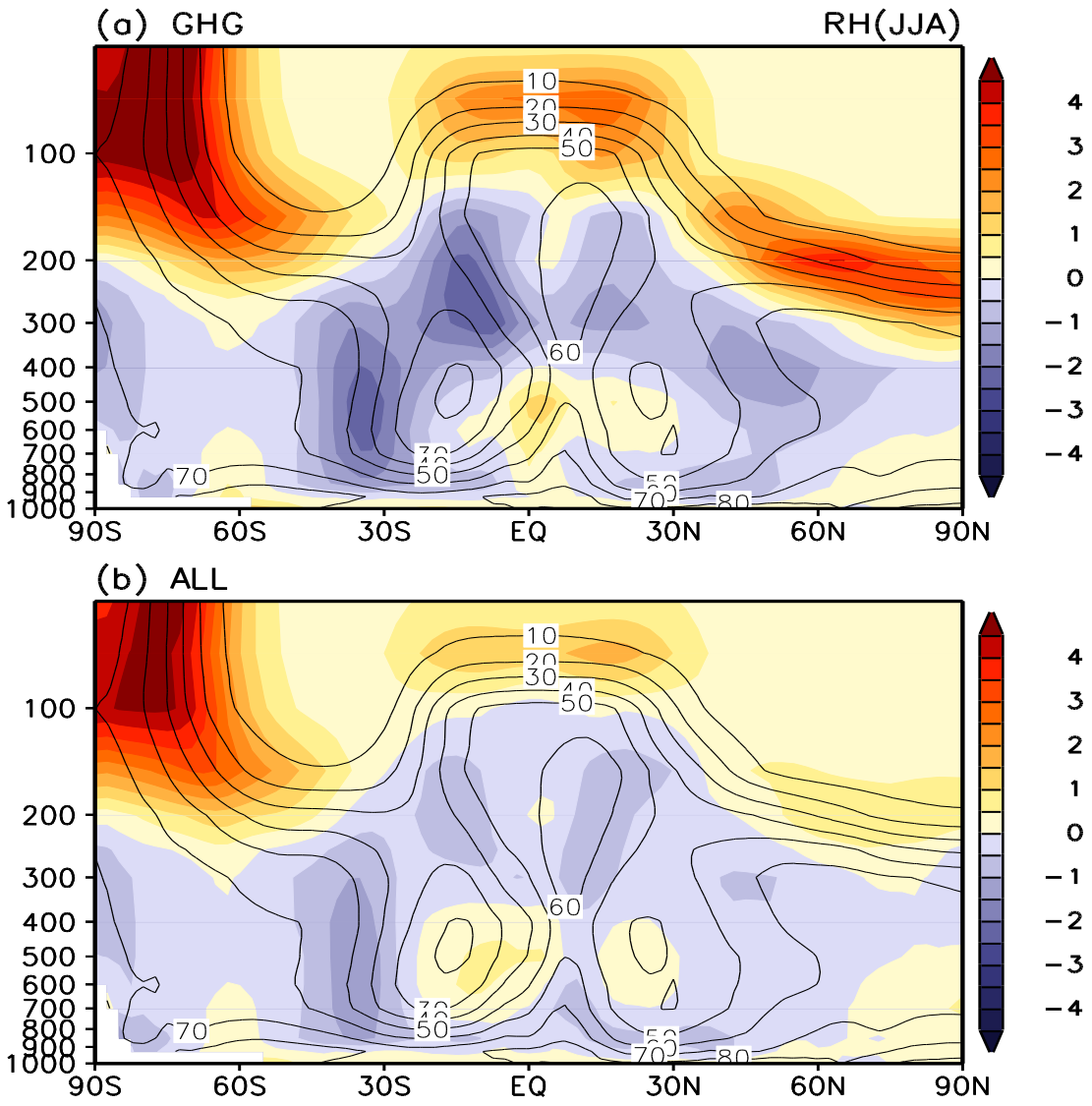
(a) GHG
RH(JJA)
(b) ALL
100
200
300
400
500
600
700
800
900
1000
90S
60S
30S
EQ
30N
60N
90N
10
20
30
40
50
60
70
80
4
3
2
1
0
−1
−2
−3
−4

Figure 2

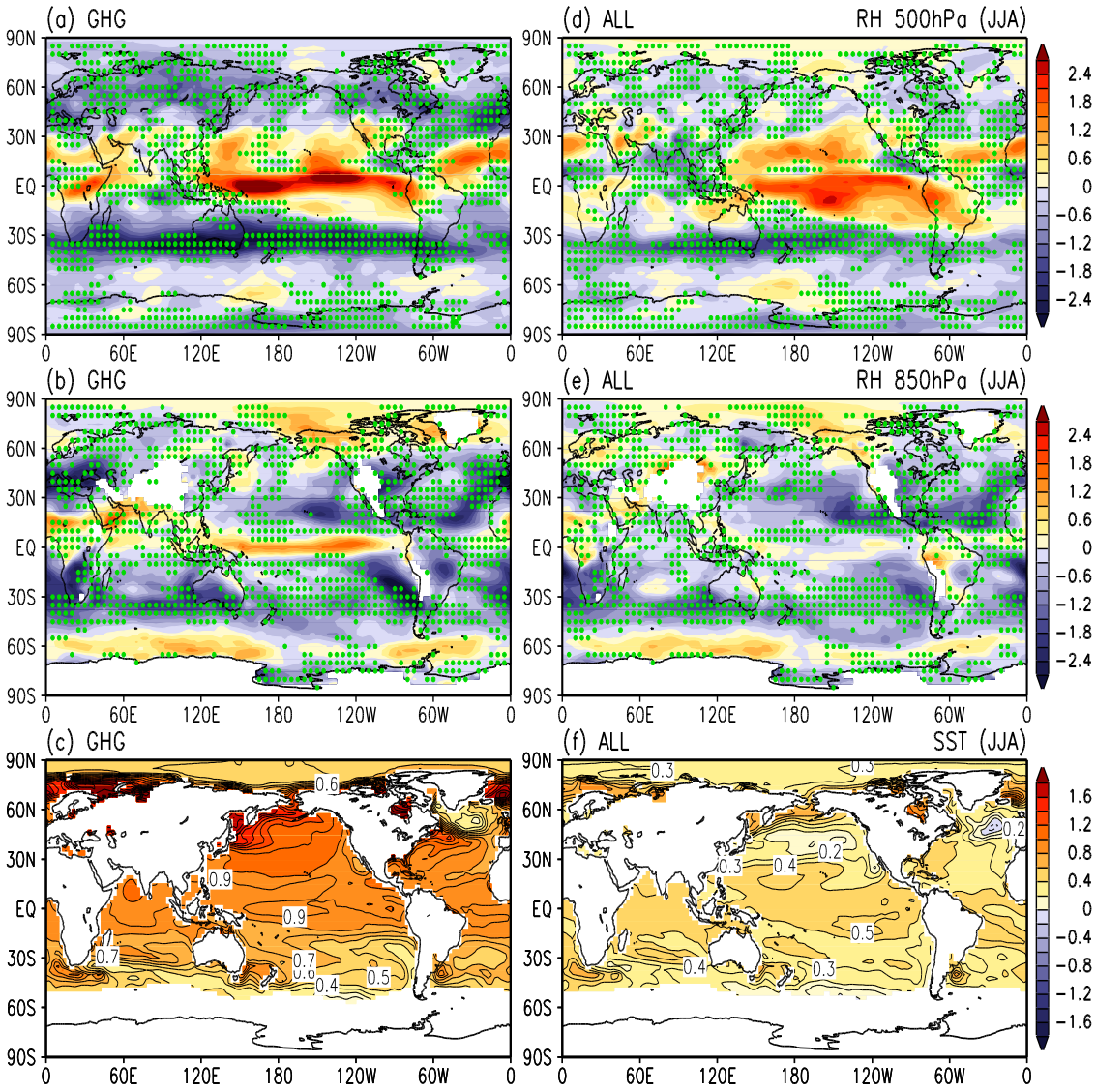
(a) GHG
(d) ALL
RH 500hPa (JJA)
(b) GHG
(e) ALL
RH 850hPa (JJA)
(c) GHG
(f) ALL
SST (JJA)
90N
60N
30N
EQ
30S
60S
90S
0
60E
120E
180
120W
60W
2.4
1.8
1.2
0.6
0
−0.6
−1.2
−1.8
−2.4
1.6
0.8
0.4
−0.4
−0.8

Figure 3

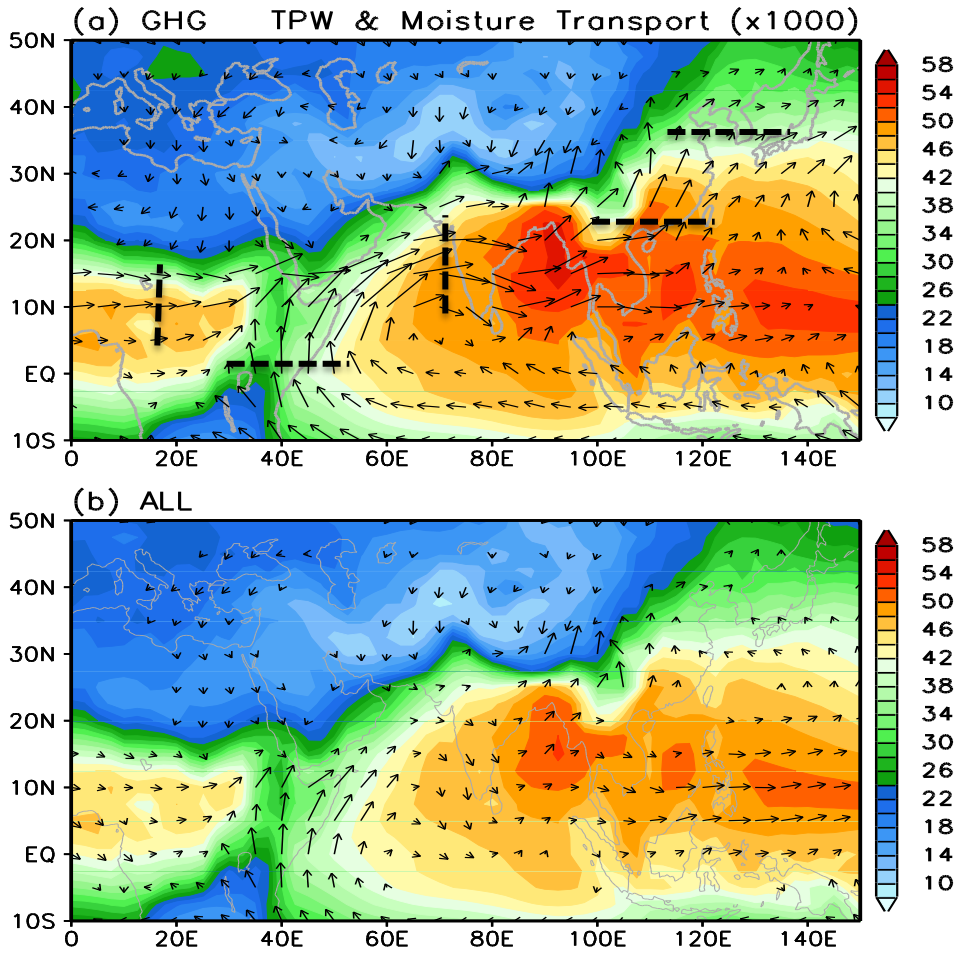
(a) GHG TPW & Moisture Transport (x1000)
50N
40N
30N
20N
10N
EQ
10S
0
20E
40E
60E
80E
100E
120E
140E
58
54
50
46
42
38
34
30
26
22
18
14
10
(b) ALL
50N
40N
30N
20N
10N
EQ
10S
0
20E
40E
60E
80E
100E
120E
140E
58
54
50
46
42
38
34
30
26
22
18
14
10

Figure 4

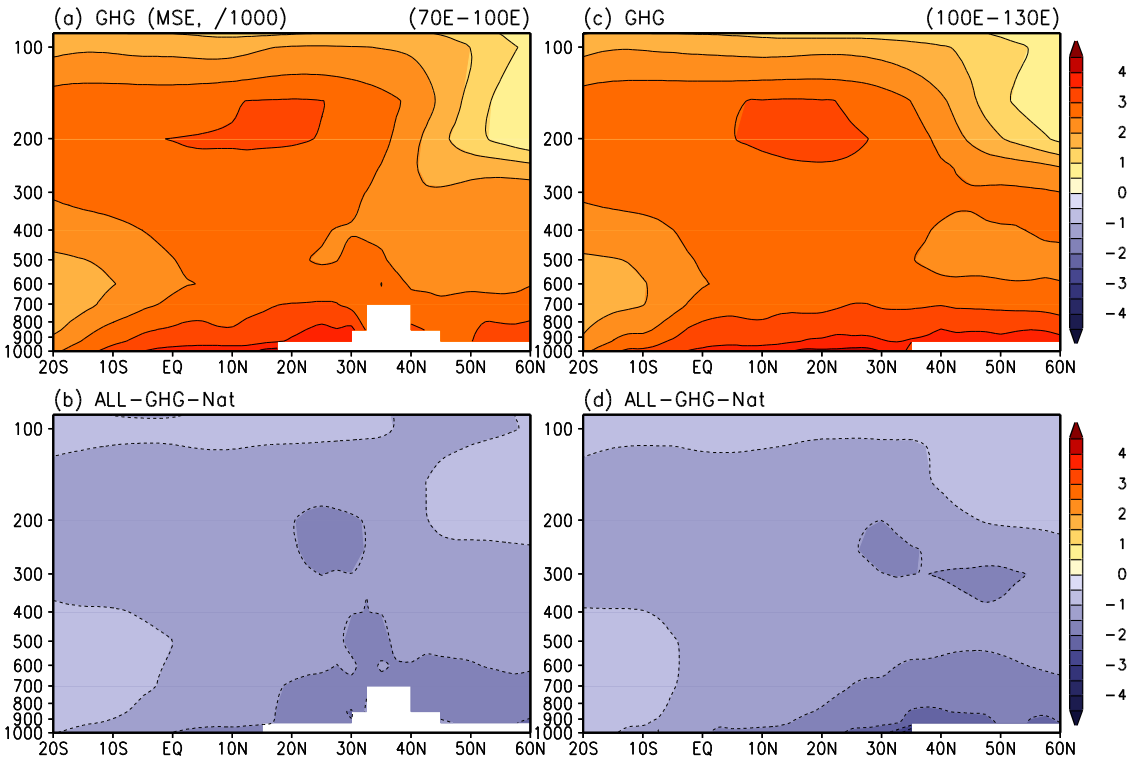
(a) GHG (MSE, /1000)
(70E−100E)
(c) GHG
(100E−130E)
(b) ALL−GHG−Nat
(d) ALL−GHG−Nat
100
200
300
400
500
600
700
800
900
1000
20S
10S
EQ
10N
20N
30N
40N
50N
60N
4
3
2
1
0
−1
−2
−3
−4

Figure 5

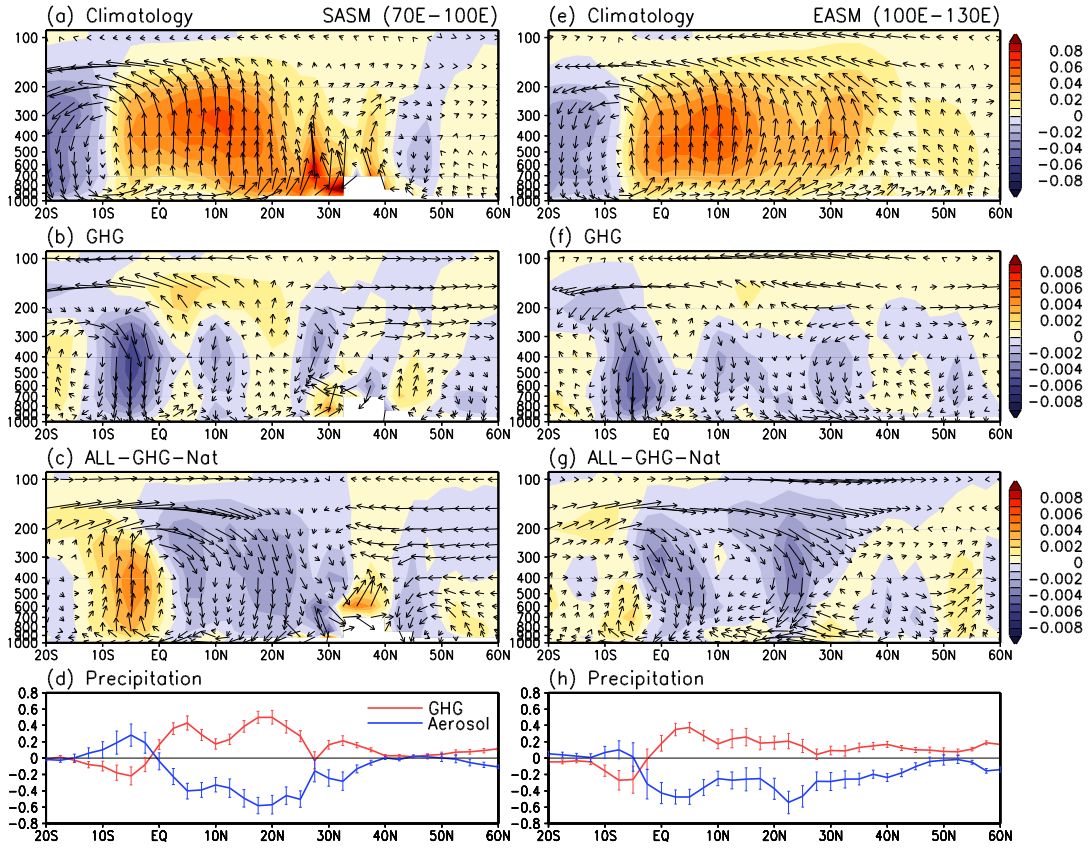
(a) Climatology
SASM (70E−100E)
(e) Climatology
EASM (100E−130E)
(b) GHG
(f) GHG
(c) ALL−GHG−Nat
(g) ALL−GHG−Nat
(d) Precipitation
(h) Precipitation
GHG
Aerosol
20S
10S
EQ
10N
20N
30N
40N
50N
60N

Figure 6

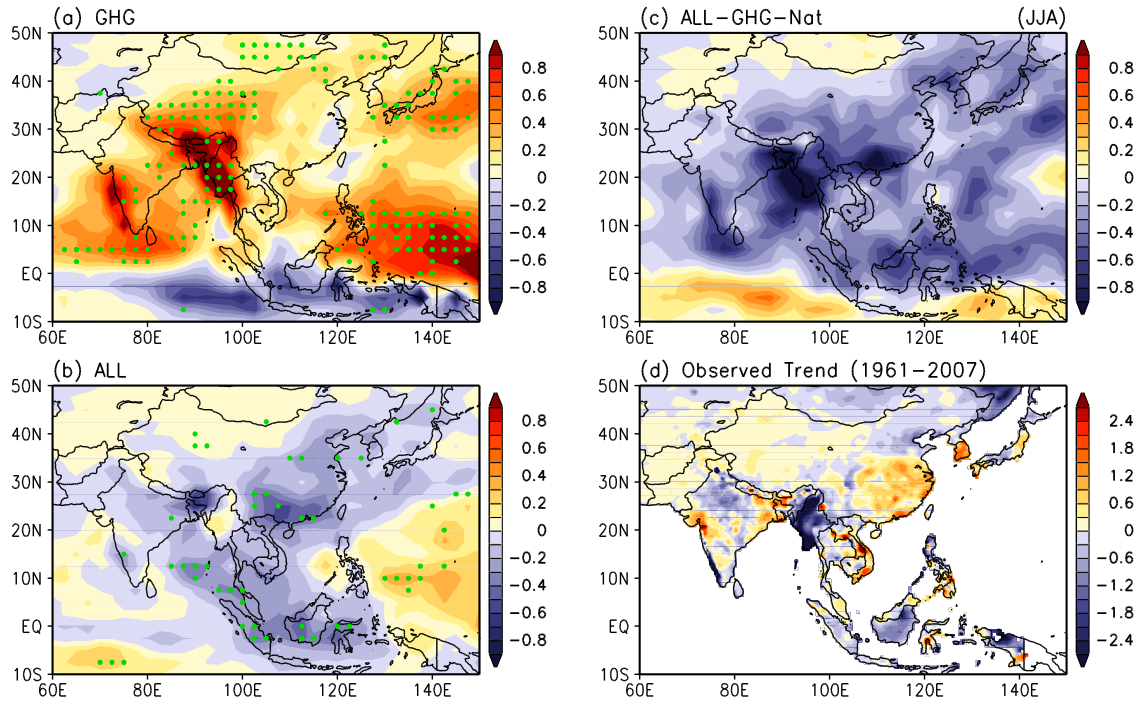
(a) GHG
(c) ALL−GHG−Nat
(JJA)
(b) ALL
(d) Observed Trend (1961−2007)
50N
40N
30N
20N
10N
EQ
10S
60E
80E
100E
120E
140E
0.8
0.6
0.4
0.2
0
−0.2
−0.4
−0.6
−0.8
2.4
1.8
1.2
0.6
0
−0.6
−1.2
−1.8
−2.4

Figure 7